FEBS Letters 585 (2011) 3947–3952

FEBS Letters

journal homepage: www.FEBSLetters.org

The *Bacillus anthracis* arylamine *N*-acetyltransferase ((BACAN)NAT1) that inactivates sulfamethoxazole, reveals unusual structural features compared with the other NAT isoenzymes ☆

Benjamin Pluvinage [a,1,3], Inés Li de la Sierra-Gallay [b,2,3], Xavier Kubiak [a], Ximing Xu [a], Julien Dairou [a], Jean-Marie Dupret [a], Fernando Rodrigues-Lima [a,*]

[a] Univ. Paris Diderot, Sorbonne Paris Cité, Unité BFA, EAC-CNRS 4413, 75013 Paris, France
[b] Institut de Biologie Physico-Chimique, CNRS FRC550, 75005 Paris, France

ARTICLE INFO

Article history:
Received 6 October 2011
Revised 25 October 2011
Accepted 25 October 2011
Available online 2 November 2011

Edited by Stuart Ferguson

Keywords:
Xenobiotic-metabolizing enzyme
Anthrax
Cofactor-binding site
Acetylation
Loop

ABSTRACT

Arylamine *N*-acetyltransferases (NATs) are xenobiotic-metabolizing enzymes that biotransform arylamine drugs. The *Bacillus anthracis* (BACAN)NAT1 enzyme affords increased resistance to the antibiotic sulfamethoxazole through its acetylation. We report the structure of (BACAN)NAT1. Unexpectedly, endogenous coenzymeA was present in the active site. The structure suggests that, contrary to the other prokaryotic NATs, (BACAN)NAT1 possesses a 14-residue insertion equivalent to the "mammalian insertion", a structural feature considered unique to mammalian NATs. Moreover, (BACAN)NAT1 structure shows marked differences in the mode of binding and location of coenzymeA when compared to the other NATs. This suggests that the mechanisms of cofactor recognition by NATs is more diverse than expected and supports the cofactor-binding site as being a unique subsite to target in drug design against bacterial NATs.

1. Introduction

Arylamine *N*-acetyltransferases (NATs: EC 2.3.1.5) are a family of enzymes that catalyze the acetylation of aromatic amines using acetyl coenzyme A (AcCoA) [1,2]. In humans, NATs play an important role in the detoxification and/or bioactivation of numerous drugs and xenobiotics [3]. These enzymes are found in a range of eukaryotic and prokaryotic species [4–7] where they may play diverse roles [6]. Determination of the structures of NATs has helped to understand the catalytic mechanisms and functions of these enzymes [6]. So far, the crystal structures of the two human NAT isoenzymes and six prokaryotic NATs have been described [8–14]. Moreover, the NMR structure of the Syrian Hamster (MESAU)NAT2 has been reported [15]. These studies identified a common fold that comprises three domains and a cysteine protease-like catalytic triad [6,16]. Although mammalian and prokaryotic NATs share the same fold, differences at the amino acid levels are known to have functional consequences [6,10,12,13,15].

Although the role of NAT in prokaryotes remains unclear, these enzymes may contribute to adaptative and/or defense mechanisms towards environmental toxins present in the habitats of bacteria [6,17]. Certain bacterial NATs are able to acetylate various aromatic amine antibiotics and increasing evidence suggests that these enzymes could contribute to antibiotic resistance in bacteria such as *Mycobaterium tuberculosis* [18,19]. In *Bacillus anthracis*, the (BACAN)NAT1 isoenzyme (formerly known as BaNATC) acetylates efficiently sulfamethoxazole and affords higher than normal resistance to this antimicrobial when expressed in *Escherichia coli* [20].

Here we present the crystal structure of (BACAN)NAT1 in complex with the cofactor coenzymeA. This novel NAT structure shows marked differences in the mode of recognition and the location of the cofactor compared to other prokaryotic and mammalian NAT enzymes. Moreover, we show that (BACAN)NAT1 possesses a 14-residues insertion equivalent to the "mammalian loop" found in human isoenzymes. This loop is likely to contribute to the shape of the active site cleft and subsequently to the recognition of the cofactor by (BACAN)NAT1, as suggested for (HUMAN)NAT2 [12,13]. By demonstrating both unexpected structural similarities

Abbreviations: NAT, arylamine *N*-acetyltransferase; SMX, sulfamethoxazole; 3′ADP, 3′ adenosine diphosphate; 5AS, 5-aminosalycilic acid; AcCoA, acetyl Coenzyme A; CoA, coenzyme A; PPi, pyrophosphate

☆ The structure has been deposited in the Protein Data Bank (PDB code 3LNB).

* Corresponding author.
E-mail address: fernando.rodrigues-lima@univ-paris-diderot.fr (F. Rodrigues-Lima).

[1] Present address: University of Victoria, Victoria, Canada.
[2] Present address: Université Paris-Sud, IBBMC, Orsay, France.
[3] BP and ILSG contributed equally to this work.

0014-5793/$36.00
doi:10.1016/j.febslet.2011.10.041

with mammalian NATs and important divergence in cofactor binding among different NAT enzymes, we provide a better understanding of the structures and functions of members within this important family of xenobiotic-metabolizing enzymes.

2. Materials and methods

2.1. Materials

Unless otherwise stated all other reagents were from Sigma–Aldrich.

2.2. Expression and purification of (BACAN)NAT1

Recombinant (BACAN)NAT1 was expressed in E.coli BL21 (DE3) and purified using nickel resin as described previously [20]. Purified (BACAN)NAT1 was dialysed against 25 mM Tris–HCl pH 7.5, 1 mM EDTA and concentrated to 8 mg/ml using ultracentrifugation concentrators (Amicon) [26].

2.3. Crystallization and data collection

Crystallization trials were performed at 294 K with AmSO4 Suite (Qiagen) and CrystalQuick microplates (Greiner). We used the hanging-drop vapour-diffusion method by mixing 1.3 μl of concentrated protein solution with 0.7 μl of reservoir solution. Microcrystals were observed after two weeks with several solutions (No. 23, 31, 37, 45). Using a mix of 2 μl of protein with 1 μl of reservoir solution, the crystallization conditions were optimized on EasyXtal Tools X-Seal (Qiagen) with 1.8 M ammonium sulphate and 0.17 M potassium nitrate. Crystals, suitable for X-ray analysis, grow in 5-7 days at a maximal size of 120 × 120 × 50 μm. They belonged to space group $P4_12_12$. For cryoprotection, the crystal was fished from the drop, put directly into sodium formate (7 M), mounted in a cryoloop (Hampton Research) and immersed into liquid nitrogen prior to X-ray diffraction analysis.

Diffraction data were collected at 100 K on the beamline ID23-1 at the ESRF using a MAR CCD detector. We used an exposure time of 0.1 s with a transmission of 16%. One thirty images were collected with 1° oscillation per image at wavelength of 0.92 Å. The data were subsequently processed with XDS [21]. The structure of (BACAN)NAT1 protein was solved at 2 Å resolution by molecular replacement, using the coordinates of *Salmonella typhimurium* NAT (PDB entry:1E2T). The atomic coordinates and structure factors have been deposited in the PDB with the accession code 3LNB. The CCP4 Software Suite was used for the structure analysis [22].

2.4. High Performance Liquid Chromatography analysis

To detect the presence of CoA in the (BACAN)NAT1 samples used for crystallisation, the protein samples were deproteinized by perchlorate (100 μl of ice-cold aqueous perchlorate (15% w/v) added to 100 μl of protein sample) and centrifugated (5 min at 12,000×*g*). The molecules present in the supernatant (20 μl) were identified by reverse-phase separation on a C18 column and Photo-Diode Array (PDA) detection. Commercialy available CoA was used as a standard.

3. Results and discussion

3.1. Overall structure

The multiple sequence alignment of (BACAN)NAT1 with several structurally and functionally characterized NATs shows that (BACAN)NAT1 shares around 30% and 20% amino acid sequence identity with bacterial and human NAT enzymes, respectively (Figs. S1 and S2). (BACAN)NAT1 contains the characteristic conserved NAT functional motifs described in all NAT enzymes characterized so far [5,23]. Moreover, the alignments also suggests that the (BACAN)NAT1 possesses an insertion of 14 amino acids at a position equivalent to the 17 amino acid insertion loop (known as the "mammalian insertion") which is considered to be specific of mammalian NATs [12,15,23,24].

Table 1
Data-collection and refinement statistics for (BACAN)NAT1 crystal.

Crystallographic data quality	
X-ray source	ID23-1, ESRF Grenoble
Wavelength (Å)	0.92
Temperature (K)	100
Unit-cell parameters (Å, °)	$a = b = 53.99$, $c = 172.44$ $\alpha = \beta = \gamma = 90$
Space group	$P4_12_12$
Resolution limits† (Å)	50.0–2.0 (2.2–2.0)
Number of observations measured†	17034 (3487)
$I/\sigma^{\dagger}(I)$	20.45 (7.91)
R_{merge}†,§ (%)	6.3 (17.7)
Overall completeness†(%)	94 (79.9)
Refinement statistics	
Number of non-hydrogen atoms (Protein/Water/CoA/Other)	2055/137/48/6
Resolution range (Å)	45.8–2.0
R/R_{free} (%)	20.3/24.4
R.M.S.D. bonds (Å)/angles (°)	0.06/1.3
Average B value-all (Å^2) Protein/Water/CoA/Other	18.85/23.68/20.26/25.06

† Values in parentheses refer to the highest resolution shell (2.2–2.0 Å).
§ $R_{merge} = \sum_h\sum_i|I_{hi}-\langle I_h\rangle|/\sum_h\sum_i I_{hi}$, were I_{hi} is the ith observation of the reflection h, while $\langle I_h\rangle$ is the mean intensity of reflection h.

The (BACAN)NAT1 crystal structure was solved by molecular replacement using the *Salmonella typhimurium* NAT structure and refined to 2 Å (Table 1). Clear electron density was present from residues 1 to 167 and from residues 183 to 267. All residues but one (Ala127) were in allowed regions of the Ramachandran plot (data not shown). More importantly, an additional electron density was found and identified as being coenzyme A (CoA) (Fig. 1). The (BACAN)NAT1 structure resembles the overall fold of eukaryotic and prokaryotic NATs [23] (Fig. 1). It consists of three domains of similar size. Domain I is an α-helical bundle (amino acids 1–84). The second domain forms a β-barrel (amino acids 85–196). The structure of 15 residues (amino acids 168–182 which encompass the 14-residues insertion) within domain II could not be determined due to lack of electron density. Domains I and II are disposed in such a way that Cys70, His108 and Asp123 form the catalytic triad (Fig. 1) [8]. The geometry of the catalytic residues is conserved between (BACAN)NAT1 and the other NAT structures with a RMSD around 0.1 Å. Domain III forms an α/β lid (amino acids 198–267). This domain shows the most variation (both in length and sequence) from the other NATs (Fig. S1) [23]. The surface of these domains presents a deep and wide active-site pocket; at the base of which the catalytic cysteine residue is found (Fig. 1). The (BACAN)NAT1 structure differs from other bacterial enzymes by RMSD values (ranging from 1.3 Å) over 183 and 217 residues for (RHILO)NAT1 and (SALTY)NAT1, respectively. Although amino acid sequence identity between (BACAN)NAT1 and human NATs is only 20%, the structure of (BACAN)NAT1 displays RMSD values of 1.4 Å over 215 residues with these enzymes.

3.2. Presence of a "mammalian-like" insertion in (BACAN)NAT1

Mammalian NATs are known to possess a 17-residue insertion ("mammalian insertion") which forms a loop between two

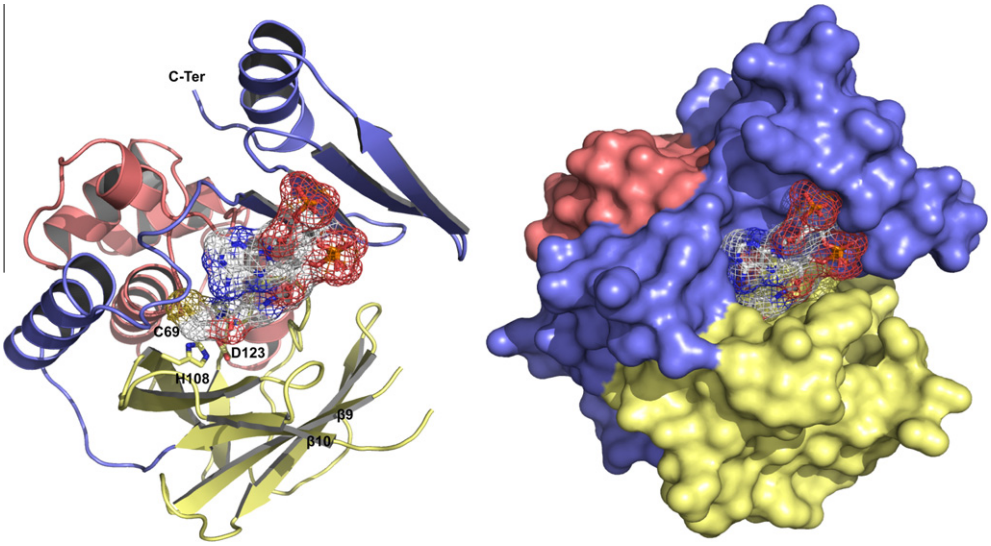

Fig. 1. X-ray crystal structure of (BACAN)NAT1. Left panel. Cartoon representation of the three-domains NAT fold of (BACAN)NAT1: helical bundle (domain I: 1-85), β-barrel (domain II: 86–197) and α/β lid (domain III: 198–267), colored in red, yellow and blue, respectively. Residues of the catalytic triad Cys^{69}-His^{108}-Asp^{123} and the co-crystallized CoA molecule are represented in sticks and electron density. β9 and β10 indicate the two β-strands flanking the 15-residues electron density gap between residue Lys^{167} and Asp^{183}. Right panel. Surface representation of BaNAT C and bound CoA (sticks and electron density).

β-strands in domain II (β9 and β11 in human NATs) [12,15,23,24]. Such an insertion is absent in the prokaryotic NAT structures reported so far where the two equivalent β-strands (β8 and β9 in (MYCMR)NAT1) are linked by a β-turn of 2–4 residues (Fig. 2) [12,23]. (BACAN)NAT1 structure reveals that an insertion of 14-amino acid (linking the β9 and β10) equivalent to the "mammalian insertion" exists in domain II of this bacterial NAT [12,16,24]. Although no electron density could be obtained, this insertion (spanning residues 169–182) is located between the β9 and β10 strands, which are structurally equivalent to β9 and β11 in (HUMAN)NAT2 (Fig. 2) [12]. The lack of electron density for this insertion in (BACAN)NAT1 was also found in a second crystal form (with characteristics similar to those of the crystal reported here i.e. space group $P4_12_12$; similar unit cell parameters; monomeric biological unit, tetragonal symmetry) (data not shown). This suggests that the insertion is highly mobile and cannot be easily resolved. In addition, SDS–PAGE and MALDI-TOF spectrometry analyses indicate that the absence of electron density for the «insertion» is not due to proteolysis. Indeed, all our SDS–PAGE analyses showed that the majority of the protein had a molecular mass around 35 kDa.

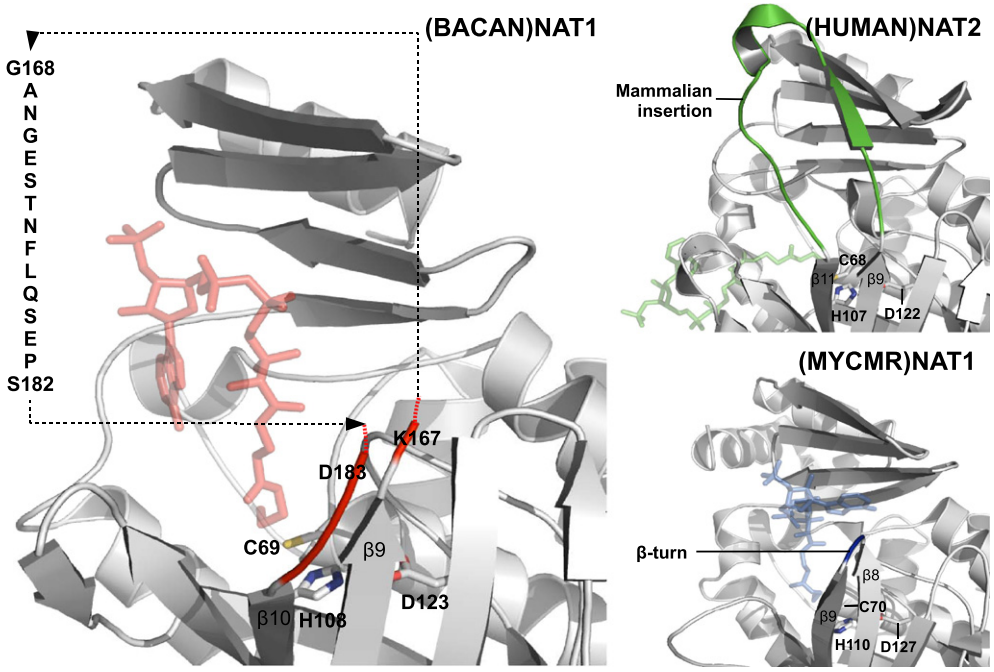

Fig. 2. Structural comparison of the "mammalian insertion" region in (HUMAN)NAT2, (BACAN)NAT1, and (MYCMR)NAT1. The three structures are superimposed and residues corresponding to the eukaryotic insertion region of (HUMAN)NAT2, (BACAN)NAT1 and (MYCMR)NAT1 are colored in green, red and blue respectively (upper panel). Lower panels depict a focus on the "mammalian-like insertion" region of (BACAN)NAT1 (red), (HUMAN)NAT2 (green) and (MYCMR)NAT1 (blue), in the same orientation, with CoA shown in transparency. In (HUMAN)NAT2, this insertion corresponds to a 17-residues loop. The corresponding aligned residues (Gly^{168}–Ser^{182}) of (BACAN)NAT1 could not be modelled and are shown as one letter codes in brackets. No "mammalian-like insertion" is present in (MYCMR)NAT1 where two strands are linked by a β-turn.

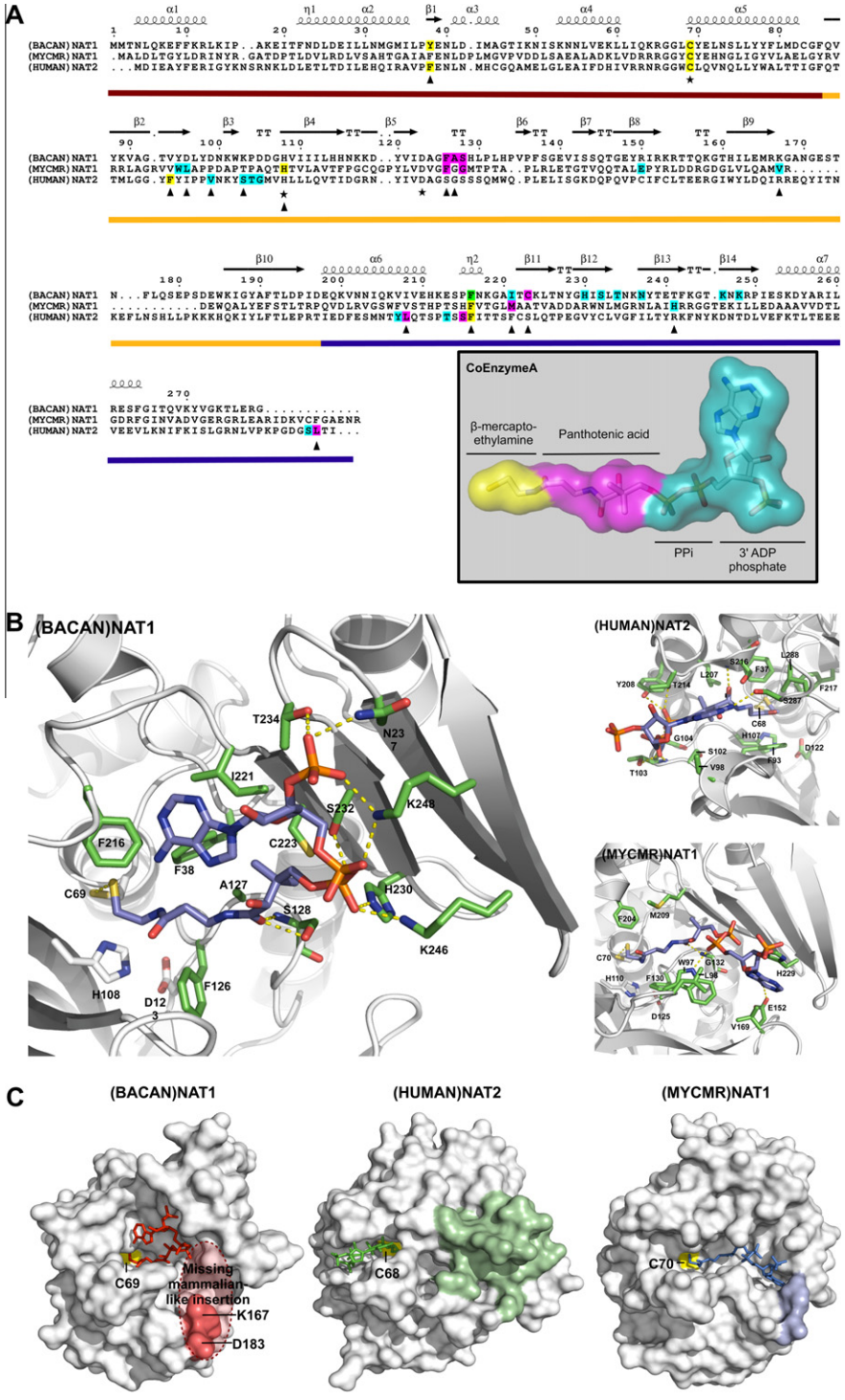

Fig. 3. Location and mode of recognition of CoA in (BACAN)NAT1, (HUMAN)NAT2 and (MYCMR)NAT1. A. Multiple amino acid sequence alignment of (BACAN)NAT1, (HUMAN)NAT2 and (MYCMR)NAT1. Catalytic residues are shown by a star and the three conserved NAT domains are represented under the alignment by a red, yellow and blue line, respectively. Residues interacting with the β-mercaptoethylamine, panthotenic acid or PPi-3′ADP phosphate part of CoA are highlighted in yellow, magenta and cyan, respectively. The green highlighted residue Phe216 of (BACAN)NAT1 interacts with both β-mercaptoethylamine and 3′ADP phosphate part of CoA. Residues labeled with a black triangle are involved in hydrophobic interactions, while the colored-only residues are forming hydrogen bonds with CoA. The structure of CoA is depicted in the lower right panel. Catalytic residues are indicated by a star. B. Amino acids involved in CoA binding are represented by green sticks (one letter code). Hydrogen bonds are shown in dots. The structure of each NAT is shown in transparency (white) and the catalytic residues are shown as white sticks. C. Surface representation of (BACAN)NAT1 (left), (HUMAN)NAT2 (middle) and (MYCMR)NAT1 (right) with the same orientation. Co-crystallized CoA molecule orientation is divergent between (BACAN)NAT1 (red sticks), HsNAT (green sticks) and (MYCMR)NAT1 (blue sticks). The catalytic cysteine is colored in yellow. The residues that flank the "mammalian-like" insertion of (BACAN)NAT1 and the region corresponding to the loop are indicated in red (left). The region corresponding of the "mammalian insertion" in (HUMAN)NAT2 is indicated in green (middle). The β-turn residues of (MYCMR)NAT1 linking the equivalent two β-strands that are linked by the insertion in (BACAN)NAT1 and human NAT2 are shown in blue.

No fragments at 22 and 11 kDa (corresponding at the removal of the insert by proteolysis) were observed. Secondly, MALDI-TOF spectrometry analyses of the protein in the crystal gave a major peak at 35514.01 Da (the theoretical mass of the protein being

35493.6 Da) (data not shown). The function of the "mammalian insertion" is not fully understood [12,24]. The structure of (HUMAN)NAT2 suggests that this insertion contributes to the shape of the enzyme active site cleft and, subsequently, to the mode of recognition of the enzyme cofactor AcCoA [12,13]. It may also contribute to the stability of the enzyme by making several contacts with other residues of the protein [12,24]. So far, (BACAN)NAT1 is the first example of a bacterial NAT that possesses a "mammalian-like" insertion.

3.3. Binding interactions and geometry of CoA in (BACAN)NAT1

As stated above, an unexpected additional electron density was found in the active site of (BACAN)NAT1 (Fig. 1). This density was identified as CoA, the non-acetylated form of AcCoA, which is the cofactor used by NATs. This result was confirmed in a second crystal (data not shown) and indicated that (BACAN)NAT1 co-crystallized with endogenous molecules of CoA that were «co-purified» with the enzyme. The presence of CoA in the (BACAN)NAT1 protein samples used for crystalisation was confirmed by reverse phase chromatography and the subsequent identification of CoA by Photo-Diode Array (PDA) spectroscopy (data not shown). Such an approach allows the rapid and precise identification of CoA based both on its retention time and its UV/visible spectrum. These data suggest that even after the purification procedure (which includes nickel-affinity chromatography and dialysis), sufficient amounts of CoA are present in the protein samples to allow the crystallization of (BACAN)NAT1 in complex with CoA. Although CoA is a product of the NAT catalyzed reaction, it is known to bind to NATs and to reduce their activity through competitive inhibition [23,25]. It is likely that (BACAN)NAT1 is more prone to crystallization when CoA is present thus explaining why only the holo-form of the enzyme was obtained. In addition, we found that (BACAN)NAT1 has a $K_{m,app}$ for AcCoA equal to 50 μM (using 5-AS as a substrate) (data not shown), which is four times lower than the $K_{m,app}$, (determined in the same conditions) for (MYCMR)NAT1 and the pseudomonas aeruginosa NAT ((PSEAE)NAT1) [13]. Contrary to (BACAN)NAT1, the other NAT-CoA cocrystals were obtained in presence of exogenous CoA [12,13].

The CoA molecule in (BACAN)NAT1 structure is mainly bound between domain II and III (Figs. 1 and 3). The binding of CoA to (MYCMR)NAT1 and (HUMAN)NAT2 was also shown to involve primarily domain II and III and similarities were indeed found with our structure. Though several key differences were found as well (Fig. 3). In (BACAN)NAT1, the majority of residues that intereact with CoA are present in the β-sheet structure of the «α/β» lid (Domain III: β11–β14). Although CoA interacts with the equivalent β-sheet in (MYCMR)NAT1, it also interacts with additional residues in two other β-sheets in domain II [13]. In (HUMAN)NAT2, the residues interacting with CoA are mainly provided by a β-sheet in domain II and by residues located in α-helices of domain III [12,13]. As found in (MYCMR)NAT1 and (HUMAN)NAT2 structures, several aromatic and aliphatic residues of (BACAN)NAT1 (such as Phe38, Phe126, Ala127, Phe216 and Ile221) make an extensive set of hydrophobic contacts throughout most of the length of the β-mercaptoethylamine and panthotenic arms of CoA (Fig. 3A and B) [12,13]. Moreover, in (BACAN)NAT1, six residues of the domain III β-sheet (His230, Ser232, Thr234, Asn237, Lys246 and Lys248) engage in several side-chain hydrogen bonds with oxygen atoms of the phosphate groups in both the pyrophosphate and phosphate 3′ADP moieties (Fig. 3A and B). Conversely, in (MYCMR)NAT1, only one residue (Lys236) of the domain III β-sheet engages in a side-chain hydrogen bond with a phosphate oxygen of the 3′ADP moiety (Fig. 3A and B) [13]. In (HUMAN)NAT2, no residue in the domain III β-sheet is involved in hydrogen bonding with CoA (Fig. 3A and B) [12].

The structure of (BACAN)NAT1 shows that three residues of the structural "P-loop" (Phe126, Ala127 and Ser128) interact with CoA (Fig. 3A and B) [8,23]. Similarly, "P-loop" residues are also involved in CoA binding in (MYCMR)NAT1 [13]. However, none of these "P-loop" residues of (BACAN)NAT1 interact with the phosphate oxygen atoms of CoA, as it had been predicted [8,13]. Also, in (HUMAN)NAT2, no interactions between the "P-loop" structure and the cofactor were found [12]. The recognition of the adenine moiety of CoA in (BACAN)NAT1 is only achieved by hydrophobic contacts (contributed by Phe38, Phe216 and Ile221) whereas in (MYCMR)NAT1 and (HUMAN)NAT2 this recognition occurs through both hydrophobic and hydrogen bonds (Fig. 3B) [12, 13].

Parts of CoA sits similarly in the cleft in (BACAN)NAT1, (MYCMR)NAT1 and (HUMAN)NAT2 such that the catalytic cysteine is close to the β-mercaptoethylamine group of CoA. Though the distal region of the cofactor interacts differently with the respective NATs (Figs. S3 and 3C and Table S1) [12,13]. This leads to marked differences in the geometry of CoA bound to the different enzymes (Figs. S3 and 3C and Table S1). In (BACAN)NAT1, the phosphate groups of the pyrophosphate segment introduce a sharp bends into the CoA molecule as a result of steric interactions between CoA and the side-chains in this region of the active site of (BACAN)NAT1 (Figs. S3 and 3C and Table S1).

In (MYCMR)NAT1 structure, the CoA molecule fits into an extended cleft that stretches for 21 Å (from the active site cysteine to the N6 atome of adenine) and over a surface of 1560 Å^2 (Fig. 3C) [13]. In (BACAN)NAT1 and (HUMAN)NAT2, the cofactor fits in an equivalent but narrower cleft that stretches for 15.9 and 9.4 Å (for (HUMAN)NAT2 and (BACAN)NAT1, respectively) over a surface of 1100 Å^2 (Fig. 3C). It has been shown that such a difference in the location and mode of binding of CoA between (MYCMR)NAT1 and (HUMAN)NAT2 is due to the shape of the cleft where the cofactor binds and, in particular, to the existence in (HUMAN)NAT2 of the "mammalian insertion." This precludes a shared mechanism of recognition of the nucleosidephosphate portion of CoA in the two NAT enzymes [13]. Although, the "mammalian-like" insertion in not observable in our (BACAN)-NAT1 structure, our data strongly suggests that this extended loop also contributes to the mode of recognition and to the location of CoA in (BACAN)NAT1 (Figs. 1 and 3C) [13]. Taken together, our results on (BACAN)NAT1 and the previously published CoA–NAT structures indicate that cofactor recognition by prokaryotic and eukaryotic NAT enzymes is likely to be more diverse than previously expected [13]. This may reflect the differing evolutionary pressures on NATs specialized for their respective roles in prokaryotes and eukaryotes.

Acknowledgments

This work was funded by grants from the Ministère de l'Enseignement Supérieur et de la Recherche (Université Paris Diderot-Paris 7) and Caisse d'Assurance Maladie des Professions Libérales-Provinces (CAMPLP). BP was supported by a fellowship from the Délégation Générale de l'Armement (DGA). XK and XX are supported by a fellowship from the Université Paris Diderot-Paris 7 and China Scholar Council, respectively. We thank Professor Edith Sim for helpful discussions and Salik Hussain and Evan Graves for reading the manuscript. We gratefully acknowledge the help of Didier Nurizzo and Ganesh Natrajan for assistance at the ESRF (Grenoble).

Appendix A. Supplementary data

Supplementary data associated with this article can be found, in the online version, at doi:10.1016/j.febslet.2011.10.041.

References

[1] Riddle, B. and Jencks, W.P. (1971) Acetyl-coenzyme A: arylamine N-acetyltransferase. Role of the acetyl- enzyme intermediate and the effects of substituents on the rate. J Biol Chem 246, 3250–3258.

[2] Dupret, J.M. and Rodrigues-Lima, F. (2005) Structure and regulation of the drug-metabolizing enzymes arylamine *N*-acetyltransferases. Curr Med Chem 12, 311–318.

[3] Hein, D. (2002) Molecular genetics and function of NAT1 and NAT2: role in aromatic amine metabolism and carcinogenesis. Mutat Res 65, 65–77.

[4] Grant, D.M., Blum, M., Beer, M. and Meyer, U.A. (1991) Monomorphic and polymorphic human arylamine N-acetyltransferases: a comparison of liver isozymes and expressed products of two cloned genes. Mol Pharmacol 39, 184–191.

[5] Rodrigues-Lima, F. and Dupret, J.M. (2002) In silico sequence analysis of arylamine N-acetyltransferases: evidence for an absence of lateral gene transfer from bacteria to vertebrates and first description of paralogs in bacteria. Biochem Biophys Res Commun 293, 783–792.

[6] Sim, E., Walters, K. and Boukouvala, S. (2008) Arylamine *N*-acetyltransferases: from structure to function. Drug Metab Rev 40, 479–510.

[7] Martins, M., Dairou, J., Rodrigues-Lima, F., Dupret, J.M. and Silar, P. (2010) Insights into the phylogeny or arylamine N-acetyltransferases in fungi. J Mol Evol 71, 141–152.

[8] Sinclair, J.C., Sandy, J., Delgoda, R., Sim, E. and Noble, M.E. (2000) Structure of arylamine *N*-acetyltransferase reveals a catalytic triad. Nat Struct Biol 7, 560–564.

[9] Sandy, J., Mushtaq, A., Kawamura, A., Sinclair, J., Noble, M. and Sim, E. (2002) The structure of arylamine N-acetyltransferase from Mycobacterium smegmatis–an enzyme which inactivates the anti-tubercular drug, isoniazid. J Mol Biol 318, 1071–1083.

[10] Westwood, I.M., Holton, S.J., Rodrigues-Lima, F., Dupret, J.-M., Bhakta, S., Noble, M.E.M. and Sim, E. (2005) Expression, purification, characterisation and structure of Pseudomonas aeruginosa arylamine N-acetyltransferase. Biochem J 385, 605–612.

[11] Holton, S.J., Dairou, J., Sandy, J., Rodrigues-Lima, F., Dupret, J.M., Noble, M.E.M. and Sim, E. (2005) Structure of Mesorhizobium loti arylamine N-acetyltransferase 1. Acta Crystallogr Sect F Struct Biol Cryst Commun 61, 14–16.

[12] Wu, H., Dombrovsky, L., Tempel, W., Martin, F., Loppnau, P., Goodfellow, G.H., Grant, D.M. and Plotnikov, A.N. (2007) Structural basis of substrate-binding specificity of human arylamine N-acetyltransferases. J Biol Chem 282, 30189–30197.

[13] Fullam, E., Westwood, I.M., Anderton, M.C., Lowe, E.D., Sim, E. and Noble, M.E. (2008) Divergence of cofactor recognition across evolution: coenzyme A binding in a prokaryotic arylamine N-acetyltransferase. J Mol Biol 375, 178–191.

[14] Martins, M., Pluvinage, B., de la Sierra-Gallay, I.L., Barbault, F., Dairou, J., Dupret, J.M. and Rodrigues-Lima, F. (2008) Functional and structural characterization of the arylamine N-acetyltransferase from the opportunistic pathogen Nocardia farcinica. J Mol Biol 383, 549–560.

[15] Zhang, N., Liu, L., Liu, F., Wagner, C.R., Hanna, P.E. and Walters, K.J. (2006) NMR-based Model Reveals the Structural Determinants of Mammalian Arylamine *N*-Acetyltransferase Substrate Specificity. J Mol Biol 363, 188–200.

[16] Grant, D.M. (2008) Structures of human arylamine N-acetyltransferases. Curr Drug Metab 9, 465–470.

[17] Rodrigues-Lima, F., Dairou, J., Diaz, C.L., Rubio, M.C., Sim, E., Spaink, H.P. and Dupret, J.M. (2006) Cloning, functional expression and characterization of Mesorhizobium loti arylamine *N*-acetyltransferases: rhizobial symbiosis supplies leguminous plants with the xenobiotic N-acetylation pathway. Mol Microbiol 60, 505–512.

[18] Bhakta, S., Besra, G.S., Upton, A.M., Parish, T., Sholto-Douglas-Vernon, C., Gibson, K.J., Knutton, S., Gordon, S., DaSilva, R.P., Anderton, M.C., et al. (2004) Arylamine *N*-acetyltransferase is required for synthesis of mycolic acids and complex lipids in Mycobacterium bovis BCG and represents a novel drug target. J Exp Med 199, 1191–1199.

[19] Sim, E., Sandy, J., Evangelopoulos, D., Fullam, E., Bhakta, S., Westwood, I., Krylova, A., Lack, N. and Noble, M. (2008) Arylamine *N*-acetyltransferases in mycobacteria. Curr Drug Metab 9, 510–519.

[20] Pluvinage, B., Dairou, J., Possot, O.M., Martins, M., Fouet, A., Dupret, J.M. and Rodrigues-Lima, F. (2007) Cloning and molecular characterization of three arylamine N-acetyltransferase genes from Bacillus anthracis: identification of unusual enzymatic properties and their contribution to sulfamethoxazole resistance. Biochemistry 46, 7069–7078.

[21] Kabsch, W. (1993) Automatic processing of rotation diffraction data from crystals of initially unknown symmetry and cell constants. J Appl Cryst 26, 795–800.

[22] Winn, M.D., Ballard, C.C., Cowtan, K.D., Dodson, E.J., Emsley, P., Evans, P.R., Keegan, R.M., Krissinel, E.B., Leslie, A.G., McCoy, A., et al. (2011) Overview of the CCP4 suite and current developments. Acta Crystallogr D Biol Crystallogr 67, 235–242.

[23] Sim, E., Lack, N., Wang, C.J., Long, H., Westwood, I., Fullam, E. and Kawamura, A. (2008) Arylamine *N*-acetyltransferases: structural and functional implications of polymorphisms. Toxicology 254, 170–183.

[24] Walraven, J.M., Trent, J.O. and Hein, D.W. (2007) Computational and experimental analyses of mammalian arylamine N-acetyltransferase structure and function. Drug Metab Dispos 35, 1001–1007.

[25] Andres, H.H., Klem, A.J., Szabo, S.M. and Weber, W.W. (1985) New spectrophotometric and radiochemical assays for acetyl-CoA: arylamine *N*-acetyltransferase applicable to a variety of arylamines. Anal Biochem 145, 367–375.

[26] Pluvinage, B., Li de la Sierra-Gallay, I., Martins, M., Ragunathan, N., Dupret, J.M. and Rodrigues-Lima, F. (2007) Crystallization and preliminary X-ray characterization of arylamine *N*-acetyltransferase C (BanatC) from *Bacillus anthracis*. Acta Crystallogr Sect F Struct Biol Cryst Commun 63, 862–864.